Biochimica et Biophysica Acta 1848 (2015) 1837–1848

Contents lists available at ScienceDirect

Biochimica et Biophysica Acta

journal homepage: www.elsevier.com/locate/bbamem

Review

Electrostatically driven lipid–protein interaction: Answers from FRET☆

Fábio Fernandes [a,1], Ana Coutinho [a,b,1], Manuel Prieto [a], Luís M.S. Loura [c,d,*]

[a] Centro de Química-Física Molecular and Institute of Nanoscience and Nanotechnology, Instituto Superior Técnico, Universidade de Lisboa, Av. Rovisco Pais, 1049-001 Lisboa, Portugal
[b] Dep. Química e Bioquímica, Faculdade de Ciências, Universidade de Lisboa, Campo Grande, 1749-016 Lisboa, Portugal
[c] Faculdade de Farmácia, Universidade de Coimbra, Pólo das Ciências da Saúde, Azinhaga de Santa Comba, 3000-548 Coimbra, Portugal
[d] Centro de Química de Coimbra, Largo D. Dinis, Rua Larga, 3004-535 Coimbra, Portugal

ARTICLE INFO

Article history:
Received 5 February 2015
Accepted 23 February 2015
Available online 11 March 2015

Keywords:
Anionic phospholipid
Fluorescence anisotropy
Förster resonance energy transfer
Membrane protein oligomerization
Model membrane system
Lipid–protein interaction

ABSTRACT

Electrostatics govern the association of a large number of proteins with cellular membranes. In some cases, these proteins present specialized lipid-binding modules or membrane targeting domains while in other cases association is achieved through nonspecific interaction of unstructured clusters of basic residues with negatively charged lipids. Given its spatial resolution in the nanometer range, Förster resonance energy transfer (FRET) is a powerful tool to give insight into protein–lipid interactions and provide molecular level information which is difficult to retrieve with other spectroscopic techniques.

In this review we present and discuss the basic formalisms of both hetero- and homo-FRET pertinent to the most commonly encountered problems in lipid–protein interaction studies and highlight some examples of implementations of different FRET methodologies to characterize lipid/protein systems in which electrostatic interactions play a crucial role. This article is part of a Special Issue entitled: Lipid–protein interactions.

Contents

Abbreviations: A, acceptor; A488, Alexa488; BAR, Bin–Amphiphysin–Rvs; BODIPY-PC, 2-(4,4-difluoro-5-methyl-4-bora-3a,4a-diaza-*s*-indacene-3-dodecanoyl)-1-hexadecanoyl-*sn*-glycero-3-phosphocholine; BRAP, breast cancer-associated protein; D, donor; DPH, 1,6-diphenyl-hexatriene; DPH-PC, 1-palmitoyl-2-[3-(diphenylhexatrienyl)propanoyl]-*sn*-glycero-3-phosphocholine; DPPC, 1,2-dipalmitoyl-*sn*-glycero-3-phosphocholine; DPPG, 1,2-dipalmitoyl-*sn*-glycero-3-phospho-*rac*-(1-glycerol); DPPS, 1,2-dipalmitoyl-*sn*-glycero-3-phosphoserine; *E*, FRET efficiency; EDANS, 5-((2-aminoethyl)amino) naphthalene-1-sulfonic acid; FITC, fluorescein isothiocyanate; FLIM, fluorescence-lifetime imaging microscopy; FRET, Förster resonance energy transfer; H0-NBAR, peptide with sequence identity to the N-terminal H0 amphipathic helix from BRAP; K_6W, hexalysyltryptophan; L/P, lipid-to-protein ratio; LUV, large unilamellar vesicles; Lz, lysozyme; NBD, nitrobenzoxadiazole; PA, phosphatidic acid; PC, phosphatidylcholine; PG, phosphatidylglycerol; PI, phosphatidylinositol; PIP, phosphatidylinositol phosphate; POPC, 1-palmitoyl,2-oleoyl-*sn*-glycero-3-phosphocholine; POPG, 1-palmitoyl,2-oleoyl-*sn*-glycero-3-phospho-*rac*-(1-glycerol); POPS, 1-palmitoyl-2-oleoyl-*sn*-glycero-3-phospho-L-serine; PS, phosphatidylserine; *R*, donor-acceptor distance; R_0, Förster radius; Rh-PE, *N*-(lissamine™-rhodamine B)-1,2-dioleoyl-*sn*-glycero-3-phosphoethanolamine; SP-B, pulmonary surfactant protein B; TOF-SIMS, time of flight-secondary ion mass spectrometry

☆ This article is part of a Special Issue entitled: Lipid-protein interactions.

* Corresponding author. Tel.: +351 239488485; fax: +351 239827126.
E-mail address: lloura@ff.uc.pt (L.M.S. Loura).

[1] Share equal first authorship.

http://dx.doi.org/10.1016/j.bbamem.2015.02.023
0005-2736/

1. The biological importance of electrostatic lipid–protein interactions

Membrane proteins are often classified on the basis of their degree of insertion in the lipid bilayer. Thus, membrane proteins deeply buried in the lipid bilayer are called integral or intrinsic, frequently spanning the membrane one or several times, whereas proteins bound to the exoplasmic or cytoplasmic periphery of the lipid bilayer are designated as peripheral. Peripheral membrane proteins can be associated with membranes through different strategies, namely by interaction with lipid headgroups, with other membrane bound proteins, or they can be covalently linked to a lipid molecule, in which case they are classified as lipid-anchored. The association of peripheral proteins with the surface of intracellular membranes is crucial for a large number of cellular functions, including signaling, membrane trafficking and cytoskeleton-membrane anchoring [1–3].

In the cases where peripheral protein association with the membrane is achieved by interaction with lipid headgroups, the nature of this association is mostly reversible and typically governed by electrostatics [4]. In some cases, these proteins present specialized lipid-binding modules or membrane targeting domains. These domains typically present positively charged pockets or surfaces, and almost exclusively have anionic phospholipids as binding partners [5]. A fraction of these domains are target-specific and bind to one specific membrane component (such as the C1, and pleckstrin homology domains) [6,7]. In other cases, association with lipid membranes is achieved through unstructured clusters of basic residues, which typically present lower specificity for interaction [8].

Anionic phospholipids such as phosphatidylserine (PS), phosphatidic acid (PA) and phosphatidylinositols (PIs), typically comprise less than 25% of membrane lipids in mammals [9]. Their distribution varies dramatically between different organelles [10], and these differences are in many cases responsible for membrane recruitment of peripheral proteins to specific subcellular locations [11]. The plasma membrane inner leaflet has the highest enrichment of acidic phospholipids, including PS, PA, PI(4)P, PI(3,4)P_2, PI(4,5)P_2, and PI(3,4,5)P_3. The concentrations of anionic lipids in this leaflet are expected to reach 30% [12], generating a strong overall negative electric field responsible for the attraction of peripheral membrane proteins with cationic patches. These electrostatic interactions are heavily dependent on factors such as ionic strength and local concentrations of charged lipids and proteins [13–15]. The binding of calcium and protein phosphorylation are also able to dramatically change localized electrostatics within the protein, and the membrane association of several peripheral membrane proteins is regulated by these two factors [13,16].

In addition, peripheral membrane proteins are able to regulate the composition, dynamics, and morphology of cellular membranes. Electrostatic sequestration of anionic lipids in the presence of membrane bound proteins has been documented for a large number of proteins [15,17]. Multivalent basic proteins generate a positive local electrostatic potential which is able to enhance the local concentration of trivalent phospholipids such as PI(4,5)P_2 (charge −4 at pH 7), even in the presence of high concentrations of monovalent acidic lipids [18].

Electrostatic sequestration by basic integral proteins generates a local enrichment of negatively charged lipids around the protein [19]. The first shell of lipids enriched around integral proteins are referred to as annular lipids as opposed to the bulk lipid population and although temporarily restricted to the protein surface, the lipid molecules interacting with the protein body are not immobile and are still in exchange with other lipids [19]. The lipid binding constants of anionic phospholipids for these annular sites have been calculated through different methodologies and were found to vary only moderately [20,21]. However, within the membrane environment, these moderate differences in affinities are expected to change the local concentrations of lipids to a significant extent [19].

Lipid molecules are also in some cases found buried within specific binding sites in the membrane protein structure. Lipids in these sites are relatively immobile and are referred to as non-annular lipids [19]. Protein activity is in some cases highly dependent on the binding of specific lipids to these sites. In the case of the potassium channel KscA, at least three non-annular binding sites have to be occupied by anionic lipids for channel opening to occur [22].

Recent accumulated evidences have also given support to the conclusion that anionic lipid membranes play an important role in amyloidogenesis. In fact, membrane surfaces, depending on their lipid composition and biophysical features, can act as an effective two-dimensional catalyst of fibrillogenesis [23,24]. The pathological conversion of amyloidogenic proteins/peptides into toxic aggregates at the membrane interface can be explained by the combined action of two main effects, namely the reduction of dimensionality and membrane-induced conformational changes. Briefly, the initial membrane partitioning step of several cationic amyloidogenic proteins/peptides is often driven by electrostatic interactions, inducing a high local peptide/protein concentration of preferentially surface-oriented/aligned molecules (Fig. 1A). In addition, the chemical heterogeneous nature of the hydrophobic–hydrophilic interface [25] makes it prone to establish all sorts of non-covalent interaction with the membrane-bound monomeric amyloidogenic peptides/proteins, promoting their conformational switch into amyloidogenic species. Upon reaching a critical surface coverage of the membrane with these aggregation-prone conformations (surface crowding effect [26]), hydrophobic interactions will promote and accelerate the cooperative formation of amyloid fibrils with a rich cross-β-sheet structure, ultimately compromising the membrane structural integrity [27,28]. As illustrated in Fig. 1B, the lipid-to-protein molar ratio (L/P) is a key parameter governing the fractional population of each species in the system, namely the aqueous and membrane-bound monomeric and oligomeric species, since membrane partitioning and self-assembly of the peptide/protein are two coupled equilibria.

Förster resonance energy transfer (FRET) is a photophysical phenomenon which depends critically on interchromophore distance. Even though the use of extrinsic labels is common, the amounts required are usually very low and non-perturbing (see examples in [29]). The spatial resolution of FRET (nanometer range) is ideal for probing a variety of processes of relevance in membrane biology. Indeed, from FRET experiments, information including extent of interaction, depth of penetration, protein oligomerization, protein/lipid selectivity and protein-induced lipid demixing or morphological alterations can be inferred and characterized. Variations in the separation and spatial arrangement of chromophores lead to alterations in FRET, that can be monitored under steady-state and/or time-resolved conditions. On a very basic level, FRET may be employed as a phenomenological indicator of molecular proximity, and a large body of work has been reported describing such qualitative applications [30]. However, to take full advantage of the technique's potential, models that describe the dependence of FRET observables on the structural properties of the system under study are required. Therefore, in this article, the basic formalisms of FRET pertinent to the most commonly encountered problems in lipid–

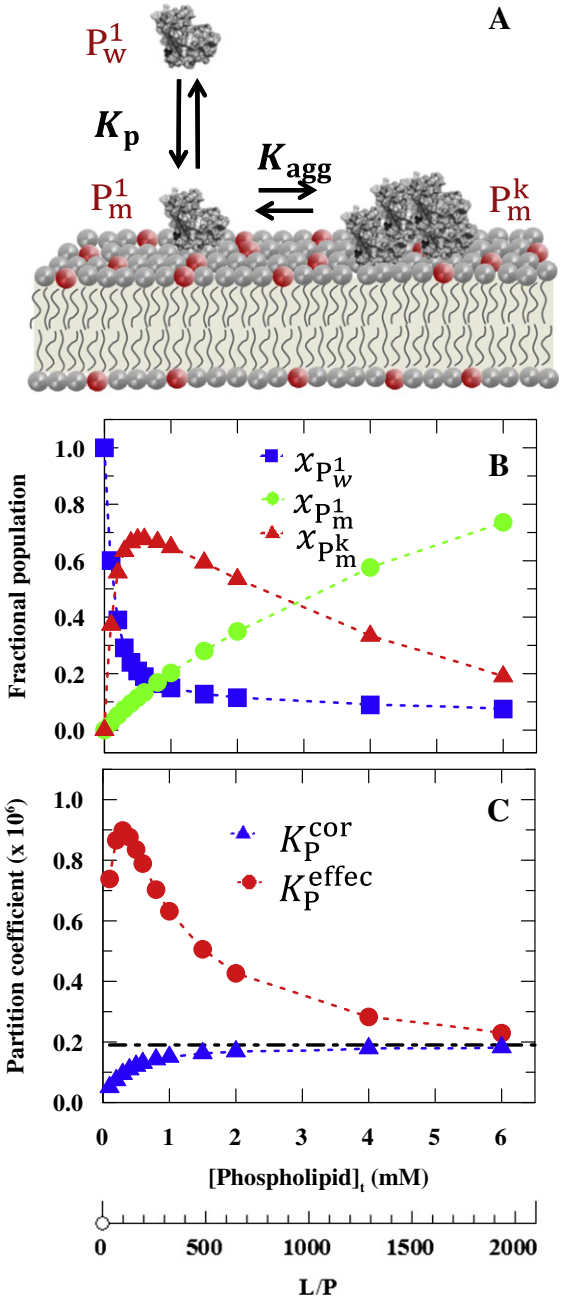

Fig. 1. Cooperative partition of peptides/proteins to anionic lipid membranes. (A) Schematic representation of a simplified three-state model of electrostatic-driven lipid–protein interaction. The zwitterionic and anionic phospholipids are represented in grey and red, respectively. (B) Upon reaching a critical surface concentration, the growth of the oligomer population (P_m^k) in the liposomes is made at the expense of the progressive recruitment of more protein monomers from the aqueous solution (P_w^1) to the membrane surface (P_m^1) since the two equilibria (membrane partition, which is governed by the partition coefficient, K_p, and reversible assembly into membrane-bound protein oligomers, controlled by the aggregation constant K_{agg}) are coupled. The total protein concentration, effective protein charge, oligomer stoichiometry and anionic lipid content used in the simulation were 3 μM, +3.5, $k = 6$ and 20 mol% POPS, respectively. (C) The intrinsic protein partition coefficient (depicted by a dashed horizontal line, $K_p = 1.9 \times 10^5$ [90,91]) decreases upon protein binding to the lipid bilayer due to the gradual screening of the interfacial membrane charge according to the Gouy–Chapman theory (blue triangles) [82]. However, the overall or effective partition coefficient, which takes into account the *k*-mers in addition to the monomeric protein recruited to the membrane, can increase several fold compared to the intrinsic protein partition coefficient when the oligomerization of membrane-bound monomeric proteins is triggered.
Adapted with permission from Melo et al., J. Phys. Chem. B 117 (2013) 2906–2917 [83]. Copyright 2013 American Chemical Society.

protein interaction are presented in Section 2. Section 3 concerns examples of studies of lipid/protein systems that were recently addressed by our group, in which electrostatic interactions play a crucial role. In all of these examples, the use of these FRET models provided detailed molecular-level information that would be virtually impossible to obtain using other experimental approaches. Together, these case studies ably illustrate the full potential of FRET in the elucidation of different aspects of lipid/protein interaction.

2. FRET formalisms

2.1. Hetero-FRET

2.1.1. Intermolecular FRET and system topological information

The phenomenon of FRET refers to the non-radiative transfer of excitation energy from one species (the donor, D) to another (the acceptor, A). It was shown by Förster [31] that it occurs with a rate constant, k_T, according to

$$k_T = \frac{1}{\tau_0}\left(\frac{R_0}{R}\right)^6. \quad (1)$$

In this equation, τ_0 is the fluorescence lifetime of D in the absence of A, R is the D–A separating distance and R_0 is a critical distance, given by

$$R_0 = 0.2108\left[\kappa^2 \Phi_0 n^{-4} \int_0^\infty \lambda^4 I(\lambda)\varepsilon(\lambda)d\lambda\right]^{1/6} \quad (2)$$

where Φ_D is the D quantum yield in the absence of A, n is the refractive index, $I(\lambda)$ is the normalized D emission spectrum, and $\varepsilon(\lambda)$ is the A molar absorption spectrum. These observables may be readily obtained from the literature or spectroscopic measurements, and pasted into a spreadsheet, such as that made available by Visser et al. [32], for convenient numerical integration. Spectral overlap of $I(\lambda)$ and $\varepsilon(\lambda)$ is a requirement for the occurrence of FRET. On the other hand, κ^2 is the so-called orientation factor, which depends on the relative D–A orientation [33]. For this parameter, the isotropic dynamic limit value (2/3) is often assumed for κ^2, although improved values can be obtained from time-resolved fluorescence anisotropy measurements [34] or simple numerical simulation, using estimates for preferred orientation and transverse location of D and A [35].

In case that D and A are distinct species (as assumed in this section), FRET from D to A is irreversible and leads to the quenching of the fluorescence of D. This is noticeable as a reduction in both its fluorescence lifetime τ and its fluorescence quantum yield Φ:

$$\frac{\tau}{\tau_0} = \frac{\Phi}{\Phi_0} = \frac{R^6}{R^6 + R_0^6}. \quad (3)$$

It must be stressed that these simple relationships only apply to (and allow the calculation of R for) situations where each D fluorophore has a single A at a reasonably close distance R (in practice, for $R < 2\,R_0$), fixed for each D–A and equal for all D–A pairs present in the ensemble. These assumptions are not met in FRET between membrane proteins and lipids, because the latter are distributed around the former, with multiple and varying D–A distances. In this complex case, the fluorescence of D is affected by the geometry of this distribution, as well as by the surface concentration of A. For each donor, the rate constant for the fluorescence decay is given by

$$k = \tau_0^{-1}\left[1 + \sum_{i=1}^{N} (R_0/R_i)^6\right] \quad (4)$$

where R_i is the distance between the donor and the i-th acceptor molecules.

Eq. (4) is the usual starting point for the derivation of D decay kinetics in membrane systems, whence relatively concise analytic solutions have been derived for the simpler geometries. For example, for planar distribution of D and A, the decay of D in the presence of A becomes [36,37]:

$$i_{DA}(t) = \exp\left(-\frac{t}{\tau_0}\right)\exp\left\{-\pi R_0^2 n_2 \gamma\left[\frac{2}{3}, \left(\frac{R_0}{R_e}\right)^6\left(\frac{t}{\tau_0}\right)\right]\left(\frac{t}{\tau_0}\right)^{1/3}\right\}\cdot \exp\left\{\pi R_e^2 n_2\left(1-\exp\left[-\left(\frac{R_0}{R_e}\right)^6\left(\frac{t}{\tau_0}\right)\right]\right)\right\} \quad (5)$$

where γ is the incomplete gamma function, R_e is the minimal D/A distance (exclusion distance) and n_2 is the surface concentration of A (molecules/unit area). Eq. (5) is valid both for a plane of A molecules containing D (*cis* transfer) and in case the D and A molecules lie in parallel planes with closest D/A distance R_e (*trans* transfer), a situation common on membranes, as D and A are often located at different depths in the bilayer. This is the basic equation for FRET in membranes, and the necessary adaptations to special D/A arrangements are relatively straightforward. For example, multiple A planes around each donor (as expected for acceptor distribution in both bilayer leaflets) requires multiplication of two exponential FRET terms, with different exclusion distances (e.g. [38]).

Although there are important advantages associated with model fitting from time-resolved data as concerned by Eq. (5) (see [38]), steady-state data obtained in a conventional spectrofluorimeter can also be used. In this case, Eq. (5) can be integrated numerically to produce FRET efficiency E values, according to

$$E = 1 - \int_0^\infty i_{DA}(t) / \int_0^\infty i_D(t) \quad (6)$$

where $i_D(t)$ is the decay of D in the absence of A. These model FRET efficiencies are compared to the experimental values obtained from

$$E = 1 - I_{DA}/I_D \quad (7)$$

where I_{DA} and I_D represent the steady-state emission intensity of D in the presence and absence of A, respectively. In this analysis, E may be calculated as a function of acceptor concentration n_2, with R_e as a parameter. Alternatively, R_e is fixed and experimental FRET decays/efficiencies are compared with theoretical expectations (with possible deviations containing useful information, e.g. protein selectivity for lipids of a certain type). Numerical integration can be carried out in a program or spreadsheet, such as that given by [39].

2.1.2. Intramolecular FRET and protein oligomerization state

The preceding section describes the kinetics of FRET between fluorescing protein and lipids. A related question that may also be addressed using FRET techniques is that of self-assembly of membrane-bound proteins. For this purpose, one may either use one or two distinctly labeled protein/peptide derivatives. In all cases, FRET may occur either to fluorophores located in the same aggregate as the donor protein (intra-aggregate FRET) or to fluorophores located elsewhere (intermolecular FRET).

We first describe here the classical approach that uses two distinctly labeled derivatives of proteins or peptides. The donor fluorescence decay in the presence of acceptors is given by [40]:

$$i_{DA}(t) = i_D(t)\left[\sum_{k=1}^{n-1} f_{Dq}(k)\rho_{bound}^{n-k}(t) + \left(1 - f_{Dq}\right)\right]\rho_{nonbound}(t) \quad (8)$$

where $f_{Dq}(k)$ is the fraction of donors bound to k acceptors (calculated according to a binomial distribution), ρ_{bound} is the FRET contribution from energy transfer to each acceptor in the same oligomer as the donor (given by $\exp(-k_T t)$, with the rate constant k_T calculated using Eq. (1)), and $\rho_{nonbound}$ is the FRET contribution arising from energy transfer to "bystander" acceptors. Traditional formalisms neglect this intermolecular term (i.e. take $\rho_{nonbound}(t) = 1$ in Eq. (8) [41–43]), which is generally only valid in the limit of very surface diluted labeled protein. To take the intermolecular term properly into account in the calculation of FRET efficiency, one should calculate $\rho_{nonbound}$ using Eq. (5) (or the variant of this equation applicable to the geometry at hand), and integrate using Eq. (6) [40]. In particular, it is inaccurate to subtract the pure intermolecular efficiency from that of combined inter-aggregate and intermolecular FRET [44]. Concerning the intra-aggregate term, several approximations have been applied, from equal energy transfer to all subunits [40–42] to zero energy transfer to distant neighbors (which is justified if the distances between them are clearly larger than R_0; [45]), whereas Li et al. [43] derived a set of equations for the case of circular ring oligomers.

2.2. Homo-FRET

In contrast to the case of different donor and acceptor, FRET between identical fluorophores (homo-FRET) does not lead to a reduction in donor fluorescence intensity or lifetime, because the donor excited state population is not diminished during the act of transfer. In practice, the sole observable which reflects the phenomenon is fluorescence anisotropy [46,47], which is reduced as a consequence of homotransfer. Despite having an obvious advantage of only requiring a single fluorophore, the use of homo-FRET is more restricted than that of hetero-FRET. The rationalization of the extent of depolarization due to homo-FRET is in fact more complicated than that of quenching due to hetero-FRET, because: i) there is the possibility of back-transfer to the directly excited donor, or transfer to any donor, eventually involving a large number of transfer steps, and ii) since fluorescence anisotropy is the relevant observable, in addition to FRET, another source of depolarization is fluorophore rotation. If rotation and FRET occur in the same timescale, the two phenomena are coupled, which constitutes the main obstacle to quantitative data analysis of homo-FRET. In this context, it is usual to neglect rotational diffusion and consider homo-FRET as the sole source of emission depolarization, or to consider rotation and energy migration as independent sources of depolarization [48].

Runnels and Scarlata [49] obtained curves for the anisotropy of clusters of varying size as a function of the reduced distance R / R_0 between monomers within the same cluster. It was assumed that fluorescence from indirectly excited monomers within an oligomer is essentially depolarized [50]. Two rotation scenarios were explored: absence of rotation, and an approximate correction based on an application of the Perrin equation to the initially-excited molecule. Both cases lead to similar results for $R / R_0 < 0.8$ (i.e. in the limit of a very efficient energy transfer among randomly oriented fluorophores within an oligomer), namely that the aggregate anisotropy is approximately given by the monomer anisotropy divided by the aggregation number.

This very simple result can be readily used in more complex situations, such as a three-state (monomer in water, monomer in membrane, oligomer in membrane) model corresponding to a coupled partition–oligomerization equilibrium (Fig. 1A) [51]. Considering the additivity law of fluorescence anisotropy and further assuming that i) the protein/peptide under study presents a fractional fluorescence labeling f, ii) the aqueous and membrane-bound monomeric molecules display the same fluorescence quantum yield but the oligomeric species is quenched by a factor $q = \Phi_{P_m^k}/\Phi_{P_m^1}$, iii) energy homotransfer is exclusively an intra-oligomeric phenomenon, iv) the occupancy level of the mixed oligomers, i.e. the fraction of i fluorescently labeled monomers per oligomer containing k subunits is described by the binomial distribution [52], and v) the anisotropy of each oligomeric species, $\langle r\rangle_{P_m^k}^i$, is inversely proportional to the number i of labeled subunits in the oligomer:

$$\langle r\rangle_{P_m^k}^i = \langle r\rangle_{P_m^k}^{i=1}/i. \quad (9)$$

Melo et al. [51] derived:

$$\langle r\rangle = \frac{x_{P_w^1}}{D}\cdot\langle r\rangle_{P_w^1} + \frac{x_{P_m^1}}{D}\cdot\langle r\rangle_{P_m^1} + \frac{\left[1-(1-f)^k\right]f^{-1}q\,x_{P_m^k}}{D}\cdot\langle r\rangle_{P_m^k}^{i=1} \quad (10)$$

with $D = x_{P_w^1} + x_{P_m^1} + k\,q\,x_{P_m^k}$. Here, $x_{P_w^1}$, $x_{P_m^1}$ and $x_{P_m^k}$ are the mole fractions of each species, $\langle r\rangle_{P_w^1}$ and $\langle r\rangle_{P_m^1}$ are the steady-state anisotropies of the monomer in aqueous solution and bound to the anionic lipid membranes (respectively) and $\langle r\rangle_{P_m^k}^{i=1}$ is the steady-state anisotropy of the oligomer containing only one labeled monomer (which cannot undergo homo-FRET). This simple analytical equation, which explicitly relates the overall steady-state anisotropy of the sample with its fractional labeling, allows to evaluate the best oligomerization stoichiometry that describes the cooperative partition equilibrium under study once the steady-state anisotropies characteristic of each fluorescent species are evaluated independently.

3. Case studies

This section illustrates the use of FRET in the study of different lipid/protein systems, based on the above described formalisms. Despite their diversity, all cases addressed below have in common a crucial role of electrostatic lipid–protein or lipid–peptide interactions (typically between negatively charged phospholipids and positively charged amino acid residues).

3.1. Pulmonary surfactant protein SP-B

Pulmonary surfactant is a lipid–protein complex responsible for reducing the surface tension of the air–liquid interface and thus prevent collapse of the alveoli at the end of expiration [53–55]. It is composed of approximately 90% of lipids and 10% of specific surfactant-associated proteins. The most abundant lipid class is zwitterionic PC, accounting for ~80% of all lipid, of which half is disaturated 1,2-dipalmitoyl-*sn*-glycero-3-phosphocholine (DPPC). Besides PC, other important phospholipid species are acidic phospholipids phosphatidylglycerol (PG), PI and PS, which together account for approximately 15% of the lipid fraction [56].

One of the four main surfactant proteins, SP-B is a 79-residue protein, containing 52% hydrophobic amino acids, and a substantial number of basic amino acids, resulting in a net charge of +5. Although it is clearly essential for surfactant homeostasis, the molecular mechanisms underlying SP-B actions are not clearly understood [57]. Although the three-dimensional structure of SP-B has not been yet determined, the protein contains about 45% α-helix, probably in the form of amphipathic helical segments [58,59]. Contradictory results have been reported with respect to the depth of penetration and the orientation of pulmonary surfactant protein SP-B in phospholipid membranes and its relative preference for interaction with anionic over zwitterionic phospholipid species. Whereas several works have suggested that SP-B is located in a shallow region of membranes, with the polar positively-charged sides of the helical segments interacting with PG, and thus causing little perturbation on the acyl chain packing of phospholipids [60–62], others have reported significant effects consistent with a deeper penetration of SP-B into the hydrophobic core [63–65]. Another matter of contention is the possibility of preferential interaction of SP-B with PG lipids, suggested by electron spin resonance data [63,66], but in contrast with TOF-SIMS analysis of lipid/protein films which seemingly indicate preferential protein partition into DPPC-enriched rather than 1,2-dipalmitoyl-*sn*-glycero-3-phospho-*rac*-(1-glycerol) (DPPG)-enriched regions [67,68].

FRET from the single tryptophan (W9) of SP-B to phospholipids of different headgroups with the NBD group attached to an acyl chain (NBD-PC, NBD-PS and NBD-PG) was used to address these questions [55]. Regarding the protein location arrangement within the 1-palmitoyl,2-oleoyl-*sn*-glycero-3-phosphocholine (POPC) membrane, two different theoretical models could be envisaged. In model I (Fig. 2A), a deep embedment of the protein in the membrane would create an area of exclusion of phospholipid molecules equivalent to the surface taken up by the protein. A topologically equivalent situation would be that originated if the protein dimer could span the whole bilayer thickness, as proposed in certain models [69]. Donor quenching by FRET in this first model could arise from two distinct acceptor populations: one located in a single circular layer of annular lipid surrounding the protein, and another uniformly distributed beyond the annular

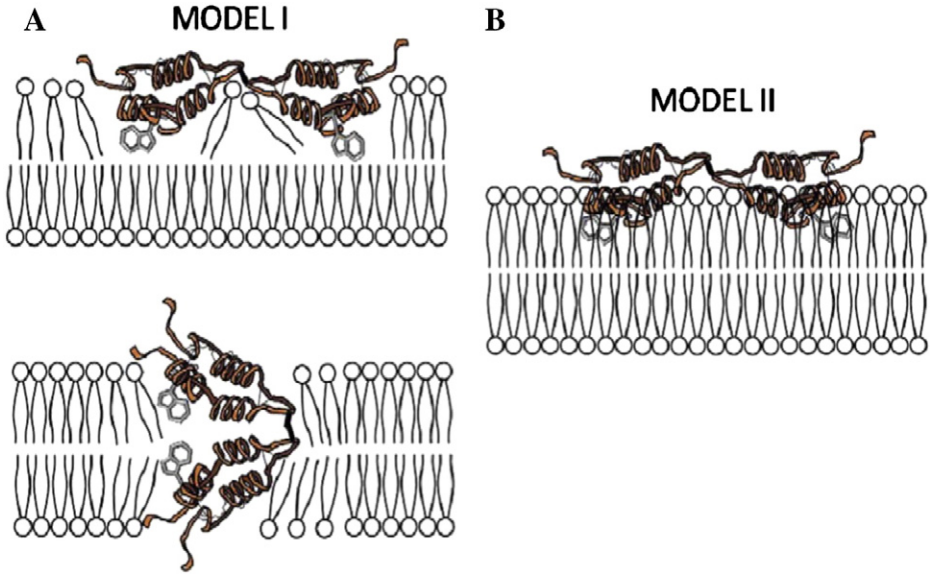

Fig. 2. Theoretical molecular models for the topology of SP-B in phospholipid membranes. Panel A represents model I, where the protein insertion leads to an excluded area in the membrane occupied by the protein instead of lipids (and therefore represents an exclusion area for FRET acceptors). Panel B represents model II, where the protein exhibits a shallow interaction with the membrane surface, with no lateral lipid excluded area. Single FRET donors (Trp residues) per SP-B monomer are indicated.
Reprinted from Biochimica et Biophysica Acta, Vol. 1818, Cabré et al., Topology and lipid selectivity of pulmonary surfactant protein SP-B in membranes: answers from fluorescence, pp. 1717–1725 [55]. Copyright 2012, with permission from Elsevier.

region. The donor decay in the presence of acceptor is thus obtained by multiplying that in absence of acceptor by the FRET terms corresponding to these two contributions [21]:

$$i_{DA}(t) = i_D(t)\rho_{annular}(t)\rho_{random}(t). \quad (11)$$

The uniform term ρ_{random} is calculated as described by Eq. (5). It was verified that the theoretical efficiency obtained with this formalism is very low when compared to the experimental measurements for reasonable values of the model parameters [55]. Therefore, this protein arrangement was discarded.

Model II (Fig. 2B) assumes that the protein adsorbs to the membrane surface. FRET can again occur to two distinct acceptor populations, one located directly below the protein (where the possibility of acceptor enrichment due to protein–lipid selectivity is considered) and another, located beyond this region (bulk bilayer). Derivation details of this model are presented elsewhere [55]. Despite the difference in topology, the main fitting parameter in this formalism is again a selectivity constant K_s, which is a measure of the preference of the protein for a given acceptor to be located underneath, over the host lipid. In particular, $K_s = 1$ denotes lack of preference for a given acceptor. As shown in Fig. 3, this model scenario still predicts less FRET efficiency than measured experimentally, even for the zwitterionic probe NBD-PC. Therefore, a moderate degree of probe preference must be invoked, as the experimental data lie between the $K_s = 1$ and $K_s = 2$ curves. This situation was found previously for the transmembrane major coat protein of bacteriophage M13 [21], and is interpreted as probably stemming from specific interactions between interfacial protein residues and the acceptor NBD group. However, this does not detract from the main conclusions: the protein is adsorbed to the bilayer surface, and a slight preference (higher K_s) is observed for anionic phospholipids PG and PS, compared to zwitterionic PC.

3.2. Helix 0 of the N-BAR domain

The members of the Bin–Amphiphysin–Rvs (BAR) domain superfamily are key membrane-sculpting proteins responsible for the generation of plasma membrane deformations. These proteins have known functions in endocytosis, vesicular transport and development of tubular membrane structures such as T-tubules of striated muscles [70]. The BAR domain is a dimeric alpha-helical protein motif, which generates a curved shape and a concave surface presenting a number of basic aminoacid residues (Fig. 4). BAR domains interact with lipid membranes

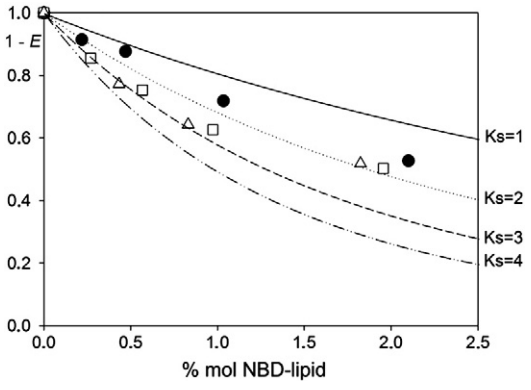

Fig. 3. Donor (SP-B W9) fluorescence quenching by FRET acceptor (NBD-lipids) in a POPC membrane matrix. Experimental time-resolved FRET data have been obtained in 50 mM Hepes, 150 mM NaCl, and pH 7.0 buffer. Acceptors were NBD-PC (closed circles), NBD-PG (squares) or NBD-PS (triangles). Lines are the theoretical curves for the different indicated selectivity constant K_s values, which consider the topology of the protein in the membrane (model II; see Fig. 2).
Reprinted from Biochimica et Biophysica Acta, Vol. 1818, Cabré et al., Topology and lipid selectivity of pulmonary surfactant protein SP-B in membranes: Answers from fluorescence, pp. 1717–1725 [55]. Copyright 2012, with permission from Elsevier.

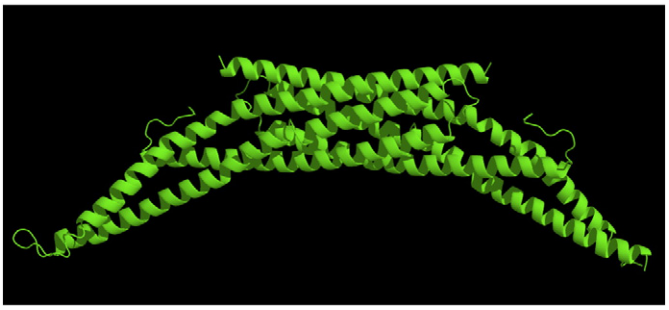

Fig. 4. Crystal structure of a dimer of BAR domains from *Drosophila* amphiphysin (PDB ID: 1URU, [71]).

through electrostatic interactions of this concave basic surface with lipid headgroups [71]. Additionally, a subset of BAR domains (N-BAR) presents a N-terminal amphipathic alpha helix (H0) which inserts in the bilayer. This subset of BAR domain proteins include amphiphysin, breast-cancer-associated protein/Bin2 (BRAP) and endophilins [72].

The membrane sculpting properties of BAR have been explained on the basis of a scaffolding mechanism, leading to the adjustment of the membrane curvature on the intrinsic shape of the protein concave surface. In the case of N-BAR domains, there is also some evidence that supports a critical role for the insertion of the H0 amphipathic helix as molecular wedge into the membrane, creating a strain in the interacting monolayer and driving curvature [71,73,74]. It has been suggested that strong hydrophobic interactions of this helix with the lipid membrane are responsible for the stabilization of the lipid bound conformation of the BAR domain.

A synthetic peptide with sequence identity to the N-terminal H0 amphipathic helix from BRAP (H0-NBAR peptide) was used to characterize the nature of the interaction of the peptide with lipid membranes. This sequence was chosen since it presents great homology to other N-terminal amphipathic helices of BAR domain-containing proteins. Binding of the peptide to the lipid bilayer is only detected for liposomes composed of anionic lipids, and after binding the peptide assumed an alpha-helical structure [40]. These results confirm that the main contribution for H0-NBAR binding to lipid membranes is electrostatic.

FRET from an EDANS (5-((2-aminoethyl)amino) naphthalene-1-sulfonic acid) labeled H0 peptide (H0-NBAR-EDANS), to different anionic phospholipids labeled with NBD at the acyl-chain (NBD-PS, NBD-PG, NBD-PA), was used to probe for specific interactions of the peptide with a particular negatively charged phospholipid. Since non-negligible liposome fusion was detected after incubation with H0-NBAR peptide, it was not possible to apply the same two-dimensional FRET formalisms (Eq. 5) for quantifying the enrichment of labeled lipids around the peptide, as done for pulmonary surfactant protein SP-B. Given this heterogeneity, only a qualitative approach can be used, and this was carried out through comparison of FRET efficiencies obtained with the different labeled phospholipid acceptors. Differences in FRET efficiencies obtained with NBD-PS, NBD-PG or NBD-PA were below 2%, within error of the measurement, pointing to a lack of selectivity of H0-NBAR-EDANS for specific anionic phospholipids [40].

Oligomerization of BAR domains within the membrane is thought to be crucial for the generation of membrane curvature. In order to determine if H0-NBAR amphipathic helices could be responsible for this oligomerization, FRET experiments between H0-NBAR-FITC and H0-NBAR-EDANS were also carried out in 1-palmitoyl,2-oleoyl-*sn*-glycero-3-phospho-*rac*-(1-glycerol) (POPG) bilayers [40]. The high R_0 of the EDANS–FITC donor–acceptor pair (40 Å) entails a small contribution of energy transfer between nonoligomerized H0-NBAR, and this was taken into account in the analysis according to Eq. (8). FRET Experiments were carried out at different peptide concentrations to make sure that this contribution was correctly accounted for. As shown in Fig. 5, the oligomerization model that provided the best fit to the data obtained at

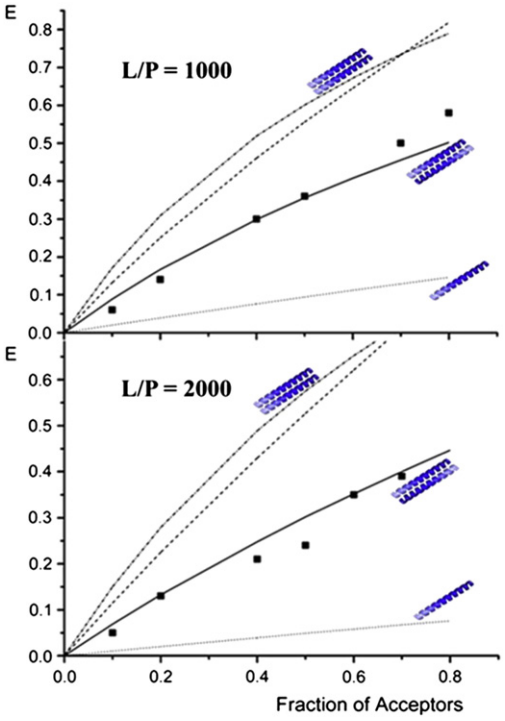

Fig. 5. H0-NBAR forms an antiparallel dimer in anionic bilayers. FRET efficiencies determined from the integration of H0-EDANS fluorescence decays in the presence of increasing fraction of acceptors (H0-FITC) (■) at a lipid-to-protein (L/P) ratio of 1000 (top panel) and 2000 (bottom panel). Simulations for FRET between monomers (dotted line), parallel dimers (dashed line) or trimers (dash-dotted line) do not describe the data accurately. The simulation which provided a more accurate description of the data was obtained for an antiparallel dimer (solid line) in which EDANS and FITC are separated by 43 Å. The maximum estimated size of H0-NBAR is 49.5 Å. These simulations take into account the contribution of FRET to nonoligomerized peptides according to Eq. (8).
Adapted from Biophysical Journal, Vol. 94, Role of Helix 0 of the N-BAR domain in membrane curvature generation, Fernandes et al., pp. 3065–3073 [40]. Copyright 2008, with permission from the Biophysical Society.

different peptide concentrations was the one that considered antiparallel dimerization of the peptide (distance of 43 Å between FITC and EDANS, close to the expected size of a fully rigid alpha-helical structure — 49.5 Å) [40].

The oligomerization of the H0-NBAR peptide explains the detection of high-order oligomers of N-BAR domains [73]. Recent results have confirmed that H0-NBAR helices do indeed arrange in antiparallel dimers, and concluded that these are essential for the assembly of the BAR domain scaffold and for the stabilization of membrane curvature [75,76].

3.3. Lysozyme as a model non-amyloidogenic protein

Recently, lysozyme (Lz) has been used as model protein to address the question of whether membranes containing acidic phospholipids can trigger rapid "amyloid-like" fiber formation by several non-amyloidogenic proteins, as proposed by [77]. Lysozyme is a small polycationic enzyme whose structure and physicochemical properties have been well characterized [78]. In addition to being widely used to study the mechanism of amyloid aggregation in vitro [78], hen egg white lysozyme is homologous to human lysozyme, whose variants have been implicated in hereditary systemic amyloidosis [79,80]. After fluorescently labeling the protein with Alexa488 (Lz-A488), a three-state cooperative partition model was first quantitatively fitted to the biphasic changes detected in its mean fluorescence lifetime in order to retrieve information about the sequential conformational/oligomerization transitions undergone by this conjugated protein upon varying its surface concentration on 1-palmitoyl-2-oleoyl-*sn*-glycero-3-phospho-L-serine (POPS)-containing liposomes (Fig. 1). By taking into account the electrostatic effects according to the Gouy–Chapman theory [81,82], Lz-A488 was found to assemble into a multimeric species (*k*-mers with $k \geq 6$) that characteristically presented a mean fluorescence lifetime shorter than the free and membrane-bound oligomeric Lz-A488 species [83]. According to the dimensions of lysozyme (a prolate ellipsoid of 3.0×4.5 nm [84]), energy homotransfer among the fluorescently labeled subunits incorporated in each mixed Lz/Lz-A488 oligomer was expected to be an efficient process, since a large Förster radius, $R_0 = 4.8$ nm, was calculated for the membrane-bound monomeric Lz-A488 at the infinite dilution regime (i.e. using a very high L/P ratio). Therefore, homo-FRET experiments were used to further narrow down the stoichiometry of the membrane-bound lysozyme oligomers by measuring the fluorescence depolarization of Lz-A488 in the presence of anionic lipid membranes. Both steady-state and time-resolved fluorescence anisotropy measurements were performed with samples presenting a variable membrane surface concentrations of Lz-A488, which was obtained by either varying the total protein or phospholipid concentrations used (Fig. 6A and B, respectively). The pronounced decrease detected in the fluorescence anisotropy of Lz-A488 was highly correlated with the extent of lysozyme oligomerization on the membrane surface, and therefore could be ascribed to an efficient intraoligomeric homo-FRET (e.g. compare Fig. 1B with Fig. 6B for 3 μM lysozyme). Additionally, incomplete labeling (variable dye-to-protein molar ratios) induced changes in homo-FRET efficiency were also explored (Fig. 6B and C, respectively). By judiciously choosing the experimental conditions that strongly displaced the oligomerization equilibrium towards the membrane-bound *k*-mers (low L/P ratio, Fig. 1B), it was found that the higher the level of occupancy of the mixed oligomers assembled at the membrane surface, the more pronounced was the decrease in the sample steady-state anisotropy due to an increase in their intraoligomeric energy homotransfer efficiency, as shown in Fig. 6C. The concomitant changes produced in the fluorescence anisotropy decays of these samples were even more dramatic, as illustrated in Fig. 6D. There was a sharp increase in the residual anisotropy, r_∞, from 0.04 to 0.22, when the fractional labeling of the sample decreased from $f = 0.54$ to $f = 0.03$. This result, which is the experimental signature for intra-oligomeric energy homotransfer [47], reflects the progressive statistical decrease of the occupancy level of the oligomer with labeled monomers. Finally, Eq. (10) was globally fitted to the steady-state anisotropy data obtained under a wide range of experimental conditions (variable anionic lipid content of the liposomes, L/P molar ratios fractional labeling of Lz (Fig. 6)) confirming that the oligomer stoichiometry of membrane-bound Lz-A488 was $k = 6 \pm 1$. A previous detailed photophysical characterization of the system under study allowed to hold $q = 0.5$, $\langle r \rangle_{P_w^1} = 0.205$, $\langle r \rangle_{P_m^1} = 0.250$ and $\langle r \rangle_{P_m^{i=1}} = 0.350$ fixed in this global analysis. This was important due to the strong correlation between several of the parameters present in our model.

In conclusion, this study illustrates the importance of carefully manipulating the experimental conditions in order to maximize the molar fractions of each fluorescent species in the system under study. This allows evaluating independently the characteristic values for the steady-state anisotropies of each fluorescent species (free monomeric protein in aqueous solution, monomeric and oligomeric membrane-bound proteins in our case), a pre-requisite to fit the fluorescence anisotropy data obtained in complex systems, like the coupled partition–oligomerization equilibrium, with Eq. (10).

3.4. Protein-induced morphological alterations of lipid vesicles

3.4.1. K_6W model peptide

For the purpose of investigating the possibility of phase separation or other morphological changes induced on mixed zwitterionic/anionic lipid mixtures by highly basic peptide/amino acid clusters in proteins, we studied the effect of the model positively charged peptide

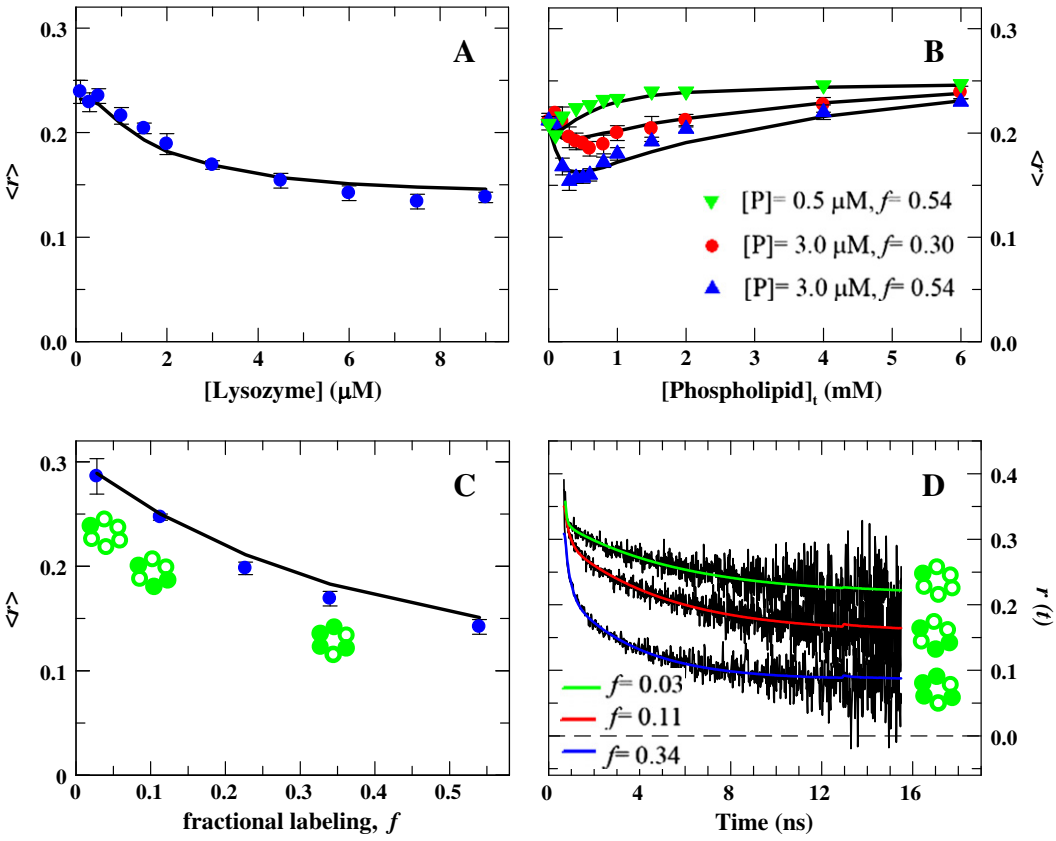

Fig. 6. Using homo-FRET to quantitatively probe the oligomerization state of membrane-bound proteins engaged in a three-state cooperative partition. Homo-FRET within the mixed membrane-bound lysozyme oligomers strongly affects the steady-state (A, B and C) and time-resolved fluorescence anisotropy (D) of Lz-A488 upon interaction with POPC:POPS 80:20 LUVs. The extent of homo-FRET critically depends on the membrane surface density of Lz-A488 (A and B) and fractional labeling, *f*, of the sample (B, C and D). The total phospholipid concentration used in A, C and D was 0.86 mM and the protein concentration employed in C and D was 6 μM. The solid black lines in A, B and C are the best fits of Eq. (10) to the steady-state anisotropy data ($k = 6$ and $K_{agg} = 2 \times 10^{14}$).
Adapted from Melo et al., Phys. Chem. Chem. Phys. 16 (2014) 18,105–18,117 [51] — Reproduced by permission of the PCCP Owner Societies.

hexalysyltryptophan (K_6W) on the organization of fluid ($T = 60$ °C) large unilamellar vesicles composed of an equimolar mixture (750 μM total lipid) of zwitterionic DPPC and anionic 1,2-dipalmitoyl-*sn*-glycero-3-phosphoserine (DPPS) [85]. In this study, rather than use FRET from the peptide to labeled lipids, a different experimental approach was used, employing two fluorescent PC lipid probes: 1-palmitoyl-2-[3-(diphenylhexatrienyl)propanoyl]-*sn*-glycero-3-phosphocholine (DPH-PC; D), and 1-palmitoyl-2-[12-(7-nitrobenz-2-oxa-1,3-diazol-4-yl) aminododecanoyl]-*sn*-glycero-3-phosphocholine (NBD-PC; A). With this setup we intended to observe whether addition of K_6W to DPPC/DPPS vesicles would increase FRET efficiency, possibly as the result of formation of PS-rich lipid domains (to which the peptide would preferentially bind), surrounded by PC-enriched membrane regions (where the FRET D and A probes would preferentially locate, with average closer separation distances).

Following our expectations, FRET in peptide-free vesicles could be analyzed with a bilayer geometry model (Fig. 7A) based on Eq. (5), and upon adding K_6W, an increase in FRET was observed. However, the latter was not due to domain formation, as analysis of decays using a modified Eq. (5) with two donor and acceptor populations (representative of PC-poor and PC-rich bilayer regions; [86]) was not successful, even for the lowest K_6W concentration used (20 μM). For $[K_6W] \leq 80$ μM, statistically acceptable fits were obtained when considering a bilamellar geometry (Fig. 7B), which would result from peptide-mediated aggregation of two bilayers. However, for higher concentrations of peptide (up to 150 μM), this model could no longer describe the experimental decays, and adequate fitting required consideration of a multilayer model (Fig. 7C), corresponding to stacked lipid bilayers with peptide sandwiched between them, and a converging value $h_2 = 4.0$ nm was recovered for sufficiently high $[K_6W]$.

It was therefore concluded that the most striking effect of this short polylysine peptide upon DPPC/DPPS equimolar mixtures is the aggregation of DPPC/DPPS vesicles, caused by the strong electrostatic interaction between the membranes' anionic groups and the basic peptide. When peptide binding reaches saturation (at ~100 μM in our experiments), there is extensive formation of stacked lipid bilayers, bridged by the anionic peptide, and with a reduced interbilayer separation of $\sim h_2 - h_1 = 2.3$ nm.

3.4.2. Lysozyme

The work with the basic model peptide described in the previous section acted as a springboard for a more extensive study, which focused on the interaction of wild-type or fluorescently-labeled lysozyme with fluid POPC/POPS vesicles. In an early stage of this study, FRET between lipid PC probes 2-(4,4-difluoro-5-methyl-4-bora-3a,4a-diaza-*s*-indacene-3-dodecanoyl)-1-hexadecanoyl-*sn*-glycero-3-phosphocholine (BODIPY-PC; D) and *N*-(lissamine™-rhodamine B)-1,2-dioleoyl-*sn*-glycero-3-phosphoethanolamine (Rh-PE; A) was measured [87]. In the absence of lysozyme, the donor decay could be analyzed using the single bilayer model based on Eq. (5). Adding increasing amounts of protein, a small but significant increase in FRET efficiency is observed for 1.0 μM < [lysozyme] < 2.0 μM, concomitant with an extensive increase in turbidity of the lipid suspension. For [lysozyme] ≥ 1.0 μM, analysis of donor decay in the presence of acceptor was significantly improved by allowing a third plane of acceptors, located at a distance h_3, which value converges to 6.7 nm in the saturation limit. This is

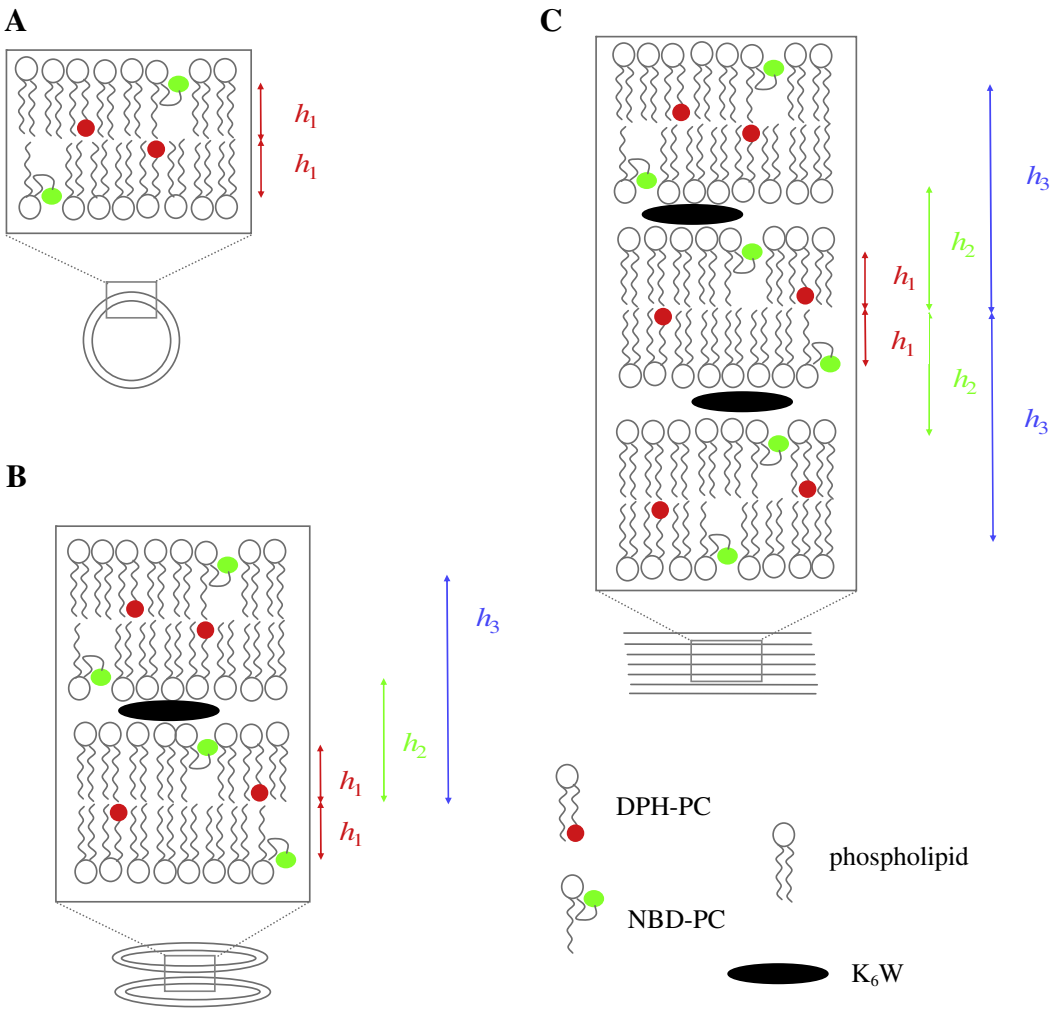

Fig. 7. Schematic diagrams of bilayer-based structures considered in the FRET models, illustrative of the interaction between K_6W and DPPC/DPPS vesicles. (A) *Bilayer geometry*: Two planes of acceptors (NBD-PC) per donor plane (DPH-PC), both at distance h_1. (B) *Bilamellar geometry*: for each donor plane, there are two acceptor planes at distance h_1 and a single acceptor plane at distance h_2. The additional plane at distance h_3 was neglected in the analysis. (C) *Multilayer geometry*: for each donor plane, there are now two acceptor planes at distances h_1 and h_2, respectively. The two acceptor planes at distance h_3 were also neglected in the analysis. B and C depict situations corresponding to peptide-induced lipid vesicle aggregation driven by electrostatic interactions. The picture is not drawn to scale.
Adapted with permission from Loura et al., J. Phys. Chem. B 110 (2006) 8130–8141 [87]. Copyright 2006 American Chemical Society.

consistent with a multilayer arrangement with a lamellar repeat distance of ≅9–10.5 nm.

In an alternate experimental setup, FRET between wild-type and 1,6-diphenyl-hexatriene, DPH, or between Alexa-488-labeled lysozyme and Rh-PE, was measured and analyzed with both single bilayer and aggregated bilayer models. Again, a transition was observed, but at slightly lower protein concentrations (0.5 μM < [lysozyme] < 1.5 μM range). Additionally, much smaller lamellar repeat distances were recovered (~5–7 nm) when the FRET donor was located in the protein. These results were conciliated with the BODIPY-PC/Rh-PE data on the basis of a "pinched lamellar" model for the lipid/lysozyme aggregates [87]: lysozyme would bridge two adjacent bilayers, with a local reduced lamellar repeat distance, not exceeding ~5–7 nm (as revealed by FRET from the protein). Between these "pinched regions", large pockets of water are contained, stabilized by hydration repulsion, leading to larger lamellar repeat distances, as concluded from the BODIPY-PC/Rh-PE experiments.

This system was again revisited later to obtain more detailed information about the micron-sized mesoscopic lipid–lysozyme mixed fibers produced at a low L/P ratio that have been proposed to present "amyloid-like" characteristics, as discussed above (Section 3.3) [78]. The multilamellar architecture of these mesoscopic structures was confirmed by performing complementary time-resolved FRET measurements between Lz-A488 (donor) and Rh-PE (acceptor), at both (bulk) ensemble and single-fiber microscopic level (FLIM-FRET measurements) [88]. After performing a centrifugation step to facilitate the imaging of the samples, the amplitude-weighted mean fluorescence lifetime of Lz-A488 measured by FLIM was found to present a rather uniform spatial distribution in these fibers, the mean value of the histograms decreasing from $\langle\tau\rangle_1^D = (1.67 \pm 0.13)$ ns to $\langle\tau\rangle_1^{DA} = (1.06 \pm 0.04)$ ns in the presence of the acceptor (Fig. 8A and B). The FRET efficiency obtained by the FLIM technique, E_{FRET}^{FLIM}, at the single-fiber level was therefore 0.36 ± 0.03 ($n = 3$). The FLIM technique, in which confocal laser scanning microscopy is combined with fluorescence decay acquisition over a section of an image, yields spatial resolution to a study. In addition, this is an intensity-independent technique that is much less sensitive to artifacts that can potentially interfere with intensity-based microscopic FRET measurements. However, due to low photon counts in each decay (pixel), and thus poor statistics, it is not possible to fit complex FRET topological models to the experimental data. To overcome this limitation, the fluorescence decay kinetics of Lz-A488 in the absence and in the presence of acceptors was also measured under macroscopic (bulk) conditions (*cuvette* measurements). According to the cooperative partition model used earlier to describe the interaction of Lz-A488 with anionic lipid membranes (Fig. 1), there was always a significant fraction of free Lz-A488 free in solution. Since the free donors do not undergo efficient Förster energy transfer to the

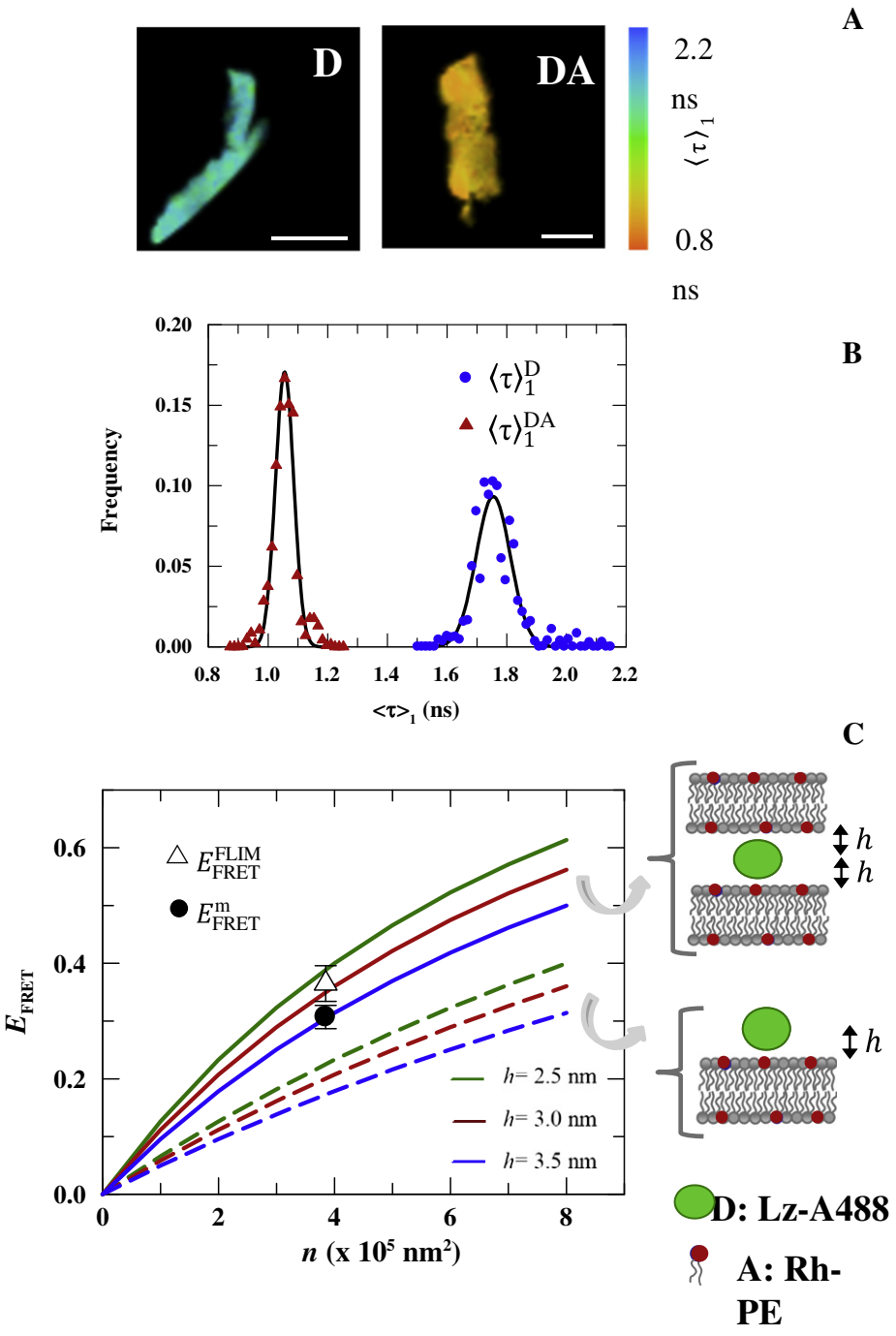

Fig. 8. The lipid–lysozyme mixed fibers produced at a low lipid/protein molar ratio display a multilayer structure. (A) Representative FLIM images of Lz-A488 in the absence (D) and presence of acceptors (DA) at the single-fiber level (scale bars represent 25 μm), and (B) the corresponding mean fluorescence lifetime, $\langle\tau\rangle_1$, histograms of the D- and DA-containing mixed lipid–protein fibers, respectively. (C) The average experimental FRET efficiencies measured both at the microscopic (E^{m}_{FRET}) and single fiber (E^{FLIM}_{FRET}) levels agree with the theoretical expectation obtained using the multilayer but not the single bilayer topological models (solid and dashed lines, respectively). The FRET efficiencies for the different acceptor surface densities, n, were simulated using an interplanar distance of $h = 2.5$ nm (green), $h = 3.0$ nm (red) and $h = 3.5$ nm (blue), respectively. The acceptor was the membrane-embedded Rh-PE.
Adapted from Melo et al., Soft matter 10 (2014) 840–850 [89] — Reproduced by permission of the Royal Society of Chemistry.

fluorescently-head labeled phospholipid used as acceptor, their presence in the solution must be accounted for in the data treatment to avoid getting underestimated FRET efficiencies [46]. As described in detail by Melo et al. [88], the interplanar FRET topological model, corrected for the presence of isolated donors in the solution, was globally fitted to a set of 3 fluorescence decays obtained for each protein concentration, namely the decay curves measured for Lz-A488 in aqueous solution, $i^{w}_{D}(t)$, and in the presence of 430 μM POPC:POPS 80:20 LUVs, including or not including the acceptor ($i_{DA}(t)$ and $i_{D}(t)$, respectively). The average bulk energy transfer efficiencies corrected for the presence of free donors in the solution $E^{m}_{FRET} = 0.31 \pm 0.02$ (mean ± SD) recovered was in good agreement with the value obtained at the single-fiber level. More importantly, both E^{m}_{FRET} and E^{FLIM}_{FRET} are also in good agreement with the interplanar energy transfer efficiency predicted for the presence of two instead of one acceptor plane (Fig. 8C) within 2.5–3.0 nm distance of membrane-bound Lz-A488, showing that lysozyme is intercalated between two adjacent lipid bilayers. These fittings presented again a low sensitivity to the transverse distance between the donor and acceptor

planes, *h*, particularly for low *h* values. Most probably, this result stems from the intrinsic heterogeneity in the donor population (co-existence of membrane-bound monomeric and hexameric Lz-A488 species; non-specific labeling of lysozyme), which is expected to broaden significantly the range of possible *h* values as mentioned before [87]. Nevertheless, the thickness of the interbilayer aqueous space, $\delta_w = 2 \times h$ ~5–6 nm, recovered in this study is now closer to the value measured earlier by performing FRET measurements between two membrane probes (D = BODIPY-PC; A = Rh-PE) in the presence of lysozyme (δ_w = 6.7 nm [87]). This interbilayer thickness is wide enough to accommodate monomeric, or even oligomeric, sideways-on or headways-on membrane-bound lysozyme molecules, particularly if lysozyme partially penetrates the membrane surface at a high protein surface coverage [89]. Altogether, these complementary FRET results, performed both at the bulk (liposome ensemble-average) and microscopic (single-fiber) levels, provided important topological information about the supramolecular organization of the lipid–lysozyme mixed fibers, confirming that they display a multilayer structure, in which the predominantly hexameric lysozyme is sandwiched between two adjacent lipid bilayers. Additional infrared spectroscopic studies of lysozyme in these samples further showed that although partly oligomerized, this protein did not exhibited a rich β-sheet structure characteristic of amyloid fibrils, ruling out the hypothesis that negatively-charged lipid membranes have the general ability to trigger amyloid fibril formation of non-amyloidogenic proteins.

4. Concluding remarks

The aim of this review was to provide an overview of different implementations of FRET for the characterization of lipid/protein systems in which electrostatic interactions play a crucial role. Given its nanometer range resolution, FRET is ideally suited to characterize protein–lipid interactions. To take full advantage of the technique's potential, models that describe the dependence of both hetero and homo-FRET observables on the structural properties of the system under study are required. The application of these models in controlled experimental conditions, allows the recovering of detailed molecular level information. As exemplified through the different case-studies presented here, this information has proven to be extremely valuable for the advancement of our understating on the role of electrostatics in protein aggregation and protein–lipid interactions.

Transparency document

The Transparency document associated with this article can be found, in the online version.

Funding sources

The authors acknowledge FCT (Projects PTDC/BBB-BQB/2661/2012 and RECI/CTM-POL/0342/2012) for financial support. F.F. is a recipient of a fellowship from FCT (SFRH/BPD/64320/2009). L. M. S. L. acknowledges additional funding by FCT, project reference PEst-OE/QUI/UI0313/2014.

References

[1] M.A. Lemmon, K.M. Ferguson, C.S. Abrams, Pleckstrin homology domains and the cytoskeleton, FEBS Lett. 513 (2002) 71–76.
[2] W. Cho, R.V. Stahelin, Membrane–protein interactions in cell signaling and membrane trafficking, Annu. Rev. Biophys. Biomol. Struct. 34 (2005) 119–151.
[3] J.T. Groves, J. Kuriyan, Molecular mechanisms in signal transduction at the membrane, Nat. Struct. Mol. Biol. 17 (2010) 659–665.
[4] A. Mulgrew-Nesbitt, K. Diraviyam, J. Wang, S. Singh, P. Murray, Z. Li, L. Rogers, N. Mirkovic, D. Murray, The role of electrostatics in protein–membrane interactions, Biochim. Biophys. Acta 1761 (2006) 812–826.
[5] M.A. Lemmon, Membrane recognition by phospholipid-binding domains, Nat. Rev. Mol. Cell Biol. 9 (2008) 99–111.
[6] P. Garcia, R. Gupta, S. Shah, A.J. Morris, S.A. Rudge, S. Scarlata, V. Petrova, S. Mclaughlin, M.J. Rebecchi, The pleckstrin homology domain of phospholipase C-δ1 binds with high affinity to phosphatidylinositol 4,5-bisphosphate in bilayer membranes, Biochemistry 34 (1995) 16228–16234.
[7] M. Guerrero-Valero, C. Marin-Vicente, J.C. Gómez-Fernandez, S. Corbalan-Garcia, The C2 domains of classical PKCs are specific PtdIns(4,5)P2-sensing domains with different affinities for membrane binding, J. Mol. Biol. 371 (2007) 608–621.
[8] S. McLaughlin, D. Murray, Plasma membrane phosphoinositide organization by protein electrostatics, Nature 438 (2005) 605–611.
[9] G. Van Meer, D.R. Voelker, G.W. Feigenson, Membrane lipids: where they are and how they behave, Nat. Rev. Mol. Cell Biol. 9 (2008) 112–124.
[10] P.A. Leventis, S. Grinstein, The distribution and function of phosphatidylserine in cellular membranes, Annu. Rev. Biophys. 39 (2010) 407–427.
[11] T. Yeung, G.E. Gilbert, J. Shi, J. Silvius, A. Kapus, S. Grinstein, Membrane phosphatidylserine regulates surface charge and protein localization, Science 319 (2008) 210–213.
[12] R.V. Stahelin, J.L. Scott, C.T. Frick, Cellular and molecular interactions of phosphoinositides and peripheral proteins, Chem. Phys. Lipids 182 (2014) 3–18.
[13] J.Y. Kim, T. Shishido, X.L. Jiang, A. Aderem, S. McLaughlin, Phosphorylation, high ionic strength, and calmodulin reverse the binding of MARCKS to phospholipid vesicles, J. Biol. Chem. 269 (1994) 28214–28219.
[14] B. Davletov, O. Perisic, R.L. Williams, Calcium-dependent membrane penetration is a hallmark of the C2 domain of cytosolic phospholipase A2 whereas the C2A domain of synaptotagmin binds membranes electrostatically, J. Biol. Chem. 273 (1998) 19093–19096.
[15] J.Y. Wang, A. Gambhir, G. Hangyas-Mihalyne, D. Murray, U. Golebiewska, S. McLaughlin, Lateral sequestration of phosphatidylinositol 4,5-bisphosphate by the basic effector domain of myristoylated alanine-rich C kinase substrate is due to nonspecific electrostatic interactions, J. Biol. Chem. 277 (2002) 34401–34412.
[16] M.E. Monteiro, M.J. Sarmento, F. Fernandes, Role of calcium in membrane interactions by PI(4,5)P2-binding proteins, Biochem. Soc. Trans. 42 (2014) 1441–1446.
[17] J. Tong, L. Nguyen, A. Vidal, S.A. Simon, J.H.P. Skene, T.J. McIntosh, Role of GAP-43 in sequestering phosphatidylinositol 4,5-bisphosphate to raft bilayers, Biophys. J. 94 (2008) 125–133.
[18] S. McLaughlin, J.Y. Wang, A. Gambhir, D. Murray, PIP(2) and proteins: interactions, organization, and information flow, Annu. Rev. Biophys. Biomol. Struct. 31 (2002) 151–175.
[19] A.G. Lee, Biological membranes: the importance of molecular detail, Trends Biochem. Sci. 36 (2011) 493–500.
[20] D. Marsh, L.I. Horváth, M.J. Swamy, S. Mantripragada, J.H. Kleinschmidt, Interaction of membrane-spanning proteins with peripheral and lipid-anchored membrane proteins: perspectives from protein–lipid interactions, Mol. Membr. Biol. 19 (2002) 247–255.
[21] F. Fernandes, L.M.S. Loura, R. Koehorst, R.B. Spruijt, M.A. Hemminga, A. Fedorov, M. Prieto, Quantification of protein–lipid selectivity using FRET: application to the M13 Major Coat Protein, Biophys. J. 87 (2004) 344–352.
[22] P. Marius, M. Zagnoni, M.E. Sandison, J.M. East, H. Morgan, A.G. Lee, Binding of anionic lipids to at least three nonannular sites on the potassium channel KcsA is required for channel opening, Biophys. J. 94 (2008) 1689–1698.
[23] G.P. Gorbenko, P.K.J. Kinnunen, The role of lipid–protein interactions in amyloid-type protein fibril formation, Chem. Phys. Lipids 141 (2006) 71–82.
[24] S.M. Butterfield, L.A. Lashuel, Amyloidogenic protein–membrane interactions: mechanistic insight from model systems, Angew. Chem. Int. Ed. 49 (2010) 5628–5654.
[25] S.H. White, W.C. Wimley, A.S. Ladokhin, K. Hristova, Protein folding in membranes: determining energetics of peptide–bilayer interactions, Methods Enzymol. 295 (1998) 62–87.
[26] C. Aisenbrey, B. Bechinger, G. Gröbner, Macromolecular crowding at membrane interfaces: adsorption and alignment of membrane peptides, J. Mol. Biol. 375 (2008) 376–385.
[27] J.D. Knight, J.A. Hebda, A.D. Miranker, Conserved and cooperative assembly of membrane-bound α-helical states of islet amyloid polypeptide, Biochemistry 45 (2006) 9496–9508.
[28] J.A. Hebda, A.D. Miranker, The interplay of catalysis and toxicity by amyloid intermediates on lipid bilayers: insights form type II diabetes, Annu. Rev. Biophys. 38 (2009) 125–152.
[29] L.M.S. Loura, J.P.P. Ramalho, Recent developments in molecular dynamics simulations of fluorescent membrane probes, Molecules 16 (2011) 5437–5452.
[30] L.M.S. Loura, M. Prieto, F. Fernandes, Quantification of protein–lipid selectivity using FRET, Eur. Biophys. J. 39 (2010) 565–578.
[31] T. Förster, Experimentelle und theoretische untersuchung des zwischenmolekularen übergangs von elektrinenanregungsenergie, Z. Naturforsch. 4a (1949) 321–327.
[32] A.J.W.G. Visser, E.S. Vysotski, J. Lee, Critical transfer distance determination between FRET pairs, http://www.photobiology.info/Experiments/Biolum-Expt.html2011 (Accessed on 12 October 2014).
[33] B.W. van der Meer, D.M. van der Meer, S.S. Vogel, Optimizing the orientation factor kappa-squared for more accurate FRET measurements, in: I. Medintz, N. Hildebrandt (Eds.), FRET — Förster Resonance Energy Transfer: From Theory to Applications, Wiley-VCH, Weinheim, 2013, pp. 63–104.
[34] R.E. Dale, J. Eisinger, W.E. Blumberg, The orientational freedom of molecular probes. The orientation factor in intramolecular energy transfer, Biophys. J. 26 (1979) 161–193 (Correction in: Biophys. J. 30 (1980) 365).
[35] L.M.S. Loura, Simple estimation of Förster resonance energy transfer (FRET) orientation factor distribution in membranes, Int. J. Mol. Sci. 13 (2012) 15252–15270.
[36] B.K. Fung, L. Stryer, Surface density determination in membranes by fluorescence energy transfer, Biochemistry 17 (1978) 5241–5248.
[37] P.K. Wolber, B.S. Hudson, An analytical solution to the Förster energy transfer problem in two dimensions, Biophys. J. 28 (1979) 197–210.

[38] L.M.S. Loura, F. Fernandes, M. Prieto, Membrane microheterogeneity: Förster resonance energy transfer characterization of lateral membrane domains, Eur. Biophys. J. 39 (2010) 589–607.
[39] C. Suárez-Germà, J. Hernández-Borrell, M. Prieto, L.M.S. Loura, Modeling FRET to investigate the selectivity of lactose permease of *Escherichia coli* for lipids, Mol. Membr. Biol. 31 (2014) 120–130.
[40] F. Fernandes, L.M.S. Loura, F.J. Chichón, J.L. Carrascosa, A. Fedorov, M. Prieto, Role of helix 0 of the N-BAR domain in membrane curvature generation, Biophys. J. 94 (2008) 3065–3073.
[41] W. Veatch, L. Stryer, The dimeric nature of the gramicidin A transmembrane channel: conductance and fluorescence energy transfer studies of hybrid channels, J. Mol. Biol. 113 (1977) 89–102.
[42] B.D. Adair, D.M. Engelman, Glycophorin A helical transmembrane domains dimerize in phospholipid bilayers: a resonance energy transfer study, Biochemistry 33 (1994) 5539–5544.
[43] M. Li, L.G. Reddy, R. Bennett, N.D. Silva Jr., L.R. Jones, D.D. Thomas, A fluorescence energy transfer method for analyzing protein oligomeric structure: application to phospholamban, Biophys. J. 76 (1999) 2587–2599.
[44] M. You, E. Li, W.C. Wimley, K. Hristova, Förster resonance energy transfer in liposomes: measurements of transmembrane helix dimerization in the native bilayer environment, Anal. Biochem. 340 (2005) 154–164.
[45] P.D. Moens, D.J. Yee, C.G. dos Remedios, Determination of the radial coordinate of Cys-374 in F-actin using fluorescence resonance energy transfer spectroscopy: effect of phalloidin on polymer assembly, Biochemistry 33 (1994) 13102–13108.
[46] J.R. Lakowicz, Principles of Fluorescence Spectroscopy, Springer, New York, 2006.
[47] A.N. Bader, S. Hoetzl, E.G. Hofman, J. Voortman, P.M.P. van Bergen en Henegouwen, G. Van Meer, H.C. Gerritsen, Homo-FRET as a tool to quantify protein and lipid clustering, Phys. Chem. Chem. Phys. 12 (2011) 475–483.
[48] B. Medhage, E. Mukhtar, B. Kalman, L.B.A. Johansson, J.G. Molotkovsky, Electronic energy transfer in anisotropic systems. 5. Rhodamine lipid derivatives in model membranes, J. Chem. Soc. Faraday Trans. 88 (1992) 2845–2851.
[49] L.W. Runnels, S.F. Scarlata, Theory and application of fluorescence homotransfer to melittin oligomerization, Biophys. J. 69 (1995) 1569–1583.
[50] V.M. Agranovich, M.D. Galanin, Electronic Excitation Energy Transfer in Condensed Matter, North-Holland Publishing, New York, 1982. (pp.).
[51] A.M. Melo, A. Fedorov, M. Prieto, A. Coutinho, Exploring homo-FRET to quantify the oligomer stoichiometry of membrane-bound proteins involved in a cooperative partition equilibrium, Phys. Chem. Chem. Phys. 16 (2014) 18105–18117.
[52] E.K. Yeow, A.H.A. Clayton, Enumeration of oligomerization states of membrane proteins in living cells by homo-FRET spectroscopy and microscopy: theory and application, Biophys. J. 92 (2007) 3096–3104.
[53] J. Pérez-Gil, Structure of pulmonary surfactant membranes and films: the role of proteins and lipid–protein interactions, Biochim. Biophys. Acta 1778 (2008) 1676–1695.
[54] Y.Y. Zuo, R.A. Veldhuizen, A.W. Neumann, N.O. Petersen, F. Possmayer, Current perspectives in pulmonary surfactant—inhibition, enhancement and evaluation, Biochim. Biophys. Acta 1778 (2008) 1947–1977.
[55] E.J. Cabré, L.M.S. Loura, A. Fedorov, J. Perez-Gil, M. Prieto, Topology and lipid selectivity of pulmonary surfactant protein SP-B in membranes: answers from fluorescence, Biochim. Biophys. Acta 1818 (2012) 1717–1725.
[56] R. Veldhuizen, K. Nag, S. Orgeig, F. Possmayer, The role of lipids in pulmonary surfactant, Biochim. Biophys. Acta 1408 (1998) 90–108.
[57] T.E. Weaver, J.J. Conkright, Functions of surfactant proteins B and C, Annu. Rev. Physiol. 63 (2001) 555–578.
[58] M. Andersson, T. Curstedt, H. Jornvall, J. Johansson, An amphipathic helical motif common to tumourolytic polypeptide NK-lysin and pulmonary surfactant polypeptide SP-B, FEBS Lett. 362 (1995) 328–332.
[59] A. Cruz, C. Casals, J. Perez-Gil, Conformational flexibility of pulmonary surfactant proteins SP-B and SP-C, studied in aqueous organic solvents, Biochim. Biophys. Acta 1255 (1995) 68–76.
[60] M.R. Morrow, J. Perez-Gil, G. Simatos, C. Boland, J. Stewart, D. Absolom, V. Sarin, K.M. Keough, Pulmonary surfactant-associated protein SP-B has little effect on acyl chains in dipalmitoylphosphatidylcholine dispersions, Biochemistry 32 (1993) 4397–4402.
[61] M.A. Oosterlaken-Dijksterhuis, H.P. Haagsman, L.M. van Golde, R.A. Demel, Characterization of lipid insertion into monomolecular layers mediated by lung surfactant proteins SP-B and SP-C, Biochemistry 30 (1991) 10965–10971.
[62] G. Vandenbussche, A. Clercx, M. Clercx, T. Curstedt, J. Johansson, H. Jornvall, J.M. Ruysschaert, Secondary structure and orientation of the surfactant protein SP-B in a lipid environment. A Fourier transform infrared spectroscopy study, Biochemistry 31 (1992) 9169–9176.
[63] J. Pérez-Gil, C. Casals, D. Marsh, Interactions of hydrophobic lung surfactant proteins SP-B and SP-C with dipalmitoylphosphatidylcholine and dipalmitoylphosphatidylglycerol bilayers studied by electron spin resonance spectroscopy, Biochemistry 34 (1995) 3964–3971.
[64] A.S. Dico, J. Hancock, M.R. Morrow, J. Stewart, S. Harris, K.M. Keough, Pulmonary surfactant protein SP-B interacts similarly with dipalmitoylphosphatidylglycerol and dipalmitoylphosphatidylcholine in phosphatidylcholine/phosphatidylglycerol mixtures, Biochemistry 36 (1997) 4172–4177.
[65] K. Shiffer, S. Hawgood, H.P. Haagsman, B. Benson, J.A. Clements, J. Goerke, Lung surfactant proteins, SP-B and SP-C, alter the thermodynamic properties of phospholipids membranes: a differential calorimetry study, Biochemistry 32 (1993) 590–597.
[66] A. Cruz, D. Marsh, J. Perez-Gil, Rotational dynamics of spin-labelled surfactant-associated proteins SP-B and SP-C in dipalmitoylphosphatidylcholine and dipalmitoylphosphatidylglycerol bilayers, Biochim. Biophys. Acta 1415 (1998) 125–134.
[67] D. Breitenstein, J.J. Batenburg, B. Hagenhoff, H.J. Galla, Lipid specificity of surfactant protein B studied by time-of-flight secondary ion mass spectrometry, Biophys. J. 91 (2006) 1347–1356.
[68] M. Seifert, D. Breitenstein, U. Klenz, M.C. Meyer, H.J. Galla, Solubility versus electrostatics: what determines lipid/protein interaction in lung surfactant, Biophys. J. 93 (2007) 1192–1203.
[69] S. Zaltash, M. Palmblad, T. Curstedt, J. Johansson, B. Persson, Pulmonary surfactant protein B: a structural model and a functional analogue, Biochim. Biophys. Acta 1466 (2000) 179–186.
[70] M. Masuda, N. Mochizuki, Structural characteristics of BAR domain superfamily to sculpt the membrane, Semin. Cell Dev. Biol. 21 (2010) 391–398.
[71] B.J. Peter, H.M. Kent, I.G. Mills, Y. Vallis, P.J.G. Butler, P.R. Evans, H.T. McMahon, BAR domains as sensors of membrane curvature: the amphiphysin BAR structure, Science 303 (2004) 495–499.
[72] H.T. McMahon, J.L. Gallop, Membrane curvature and mechanisms of dynamic cell membrane remodeling, Nature 438 (2005) 590–596.
[73] K. Farsad, N. Ringstad, K. Takei, S.R. Floyd, K. Rose, P. De Camilli, Generation of high curvature membranes mediated by direct endophilin bilayer interactions, J. Cell Biol. 155 (2001) 193–200.
[74] J.L. Gallop, C.C. Jao, H.M. Kent, P.J.G. Butler, P.R. Evans, R. Langen, H.T. McMahon, Mechanism of endophilin N-BAR domain-mediated membrane curvature, EMBO J. 25 (2006) 2898–2910.
[75] H. Cui, C. Mim, F.X. Vázquez, E. Lyman, V.M. Unger, G.A. Voth, Understanding the role of amphipathic helices in N-BAR domain driven membrane remodeling, Biophys. J. 104 (2013) 404–411.
[76] C. Mim, H. Cui, J.A. Gawronski-Salerno, A. Frost, G.A. Voth, V.M. Unger, Structural basis of membrane bending by the N-BAR protein endophilin, Cell 149 (2013) 137–145.
[77] H. Zhao, E.K. Tuominen, P.K. Kinnunen, Formation of amyloid fibers triggered by phosphatidylserine-containing membranes, Biochemistry 43 (2004) 10302–10307.
[78] A.J. Trexler, M.R. Nilsson, The formation of amyloid fibrils from proteins in the lysozyme family, Curr. Protein Pept. Sci. 8 (2007) 537–557.
[79] M.B. Pepys, P.N. Hawkins, D.R. Booth, D.M. Vigushin, G.A. Tennent, A.K. Soutar, N. Totty, O. Nguyen, C.C.F. Blake, C.J. Jerry, et al., Human lysozyme gene mutations cause hereditary systemic amyloidosis, Nature 362 (1993) 553–557.
[80] D.R. Booth, M. Sunde, V. Bellotti, C.V. Robinson, W.L. Hutchinson, P.E. Fraser, P.N. Hawkins, C.M. Dobson, S.E. Radford, C.C.F. Blake, M.B. Pepys, Instability, unfolding and aggregation of human lysozyme variants underlying amyloid fibrillogenesis, Nature 385 (1997) 787–793.
[81] S. McLaughlin, The electrostatic properties of membranes, Annu. Rev. Biophys. Biophys. Chem. 18 (1989) 113–136.
[82] J. Seelig, Thermodynamics of lipid–peptide interactions, Biochim. Biophys. Acta 1666 (2004) 40–50.
[83] A.M. Melo, J.C. Ricardo, A. Fedorov, M. Prieto, A. Coutinho, Fluorescence detection of lipid-induced oligomeric intermediates involved in lysozyme "amyloid-like" fiber formation driven by anionic membranes, J. Phys. Chem. B 117 (2013) 2906–2917.
[84] C.C.F. Blake, D.F. Koenig, G.A. Mair, A.C.T. North, D.C. Philipis, V.R. Sarma, Structure of hen egg-white lysozyme — a 3-dimensional Fourier synthesis at 2 Å resolution, Nature 206 (1965) 757–761.
[85] L.M. Loura, A. Coutinho, A. Silva, A. Fedorov, M. Prieto, Structural effects of a basic peptide on the organization of dipalmitoylphosphatidylcholine/dipalmitoylphosphatidylserine membranes: a fluorescence resonance energy transfer study, J. Phys. Chem. B 110 (2006) 8130–8141.
[86] L.M.S. Loura, A. Fedorov, M. Prieto, Fluid–fluid membrane microheterogeneity: a fluorescence resonance energy transfer study, Biophys. J. 80 (2001) 776–788.
[87] A. Coutinho, L.M. Loura, A. Fedorov, M. Prieto, Pinched multilamellar structure of aggregates of lysozyme and phosphatidylserine-containing membranes revealed by FRET, Biophys. J. 95 (2008) 4726–4736.
[88] A.M. Melo, L.M.S. Loura, F. Fernandes, J. Villalaín, M. Prieto, A. Coutinho, Electrostatically driven lipid–lysozyme mixed fibers display a multilamellar structure without amyloid features, Soft Matter 10 (2014) 840–850.
[89] B. Yuan, L.L. Xing, Y.D. Zhang, Y. Lu, Y.Y. Luo, Z.H. Mai, M. Li, Penetration and saturation of lysozyme in phospholipid bilayers, J. Phys. Chem. B 111 (2007) 6151–6155.
[90] A.M. Melo, M. Prieto, A. Coutinho, Quantifying lipid–protein interaction by fluorescence correlation spectroscopy (FCS), Methods Mol. Biol. 1076 (2014) 575–595.
[91] A.M. Melo, M. Prieto, A. Coutinho, The effect of variable liposome brightness on quantifying lipid–protein interactions using fluorescence correlation spectroscopy, Biochim. Biophys. Acta 1808 (2011) 2559–2568.